

Article

Preparation, Characterization and Intermediate-Temperature Electrochemical Properties of Er³⁺-Doped Barium Cerate–Sulphate Composite Electrolyte

Fufang Wu ^{1,*}, Ruifeng Du ¹, Tianhui Hu ¹, Hongbin Zhai ² and Hongtao Wang ^{1,*} 

¹ Anhui Provincial Key Laboratory for Degradation and Monitoring of Pollution of the Environment, School of Chemical and Material Engineering, Fuyang Normal University, Fuyang 236037, China

² Guangdong Provincial Key Lab of Nano-Micro Materials Research, School of Chemical Biology and Biotechnology, Peking University Shenzhen Graduate School, Shenzhen 518055, China

* Correspondence: wff05001@fync.edu.cn (F.W.); hwang@fync.edu.cn (H.W.)

Received: 17 July 2019; Accepted: 26 August 2019; Published: 27 August 2019



Abstract: In this study, BaCe_{0.9}Er_{0.1}O_{3-α} was synthesized by a microemulsion method. Then, a BaCe_{0.9}Er_{0.1}O_{3-α}-K₂SO₄-BaSO₄ composite electrolyte was obtained by compounding it with a K₂SO₄-Li₂SO₄ solid solution. BaCe_{0.9}Er_{0.1}O_{3-α} and BaCe_{0.9}Er_{0.1}O_{3-α}-K₂SO₄-BaSO₄ were characterized by X-ray diffraction (XRD), scanning electron microscopy (SEM) and Raman spectrometry. AC impedance spectroscopy was measured in a nitrogen atmosphere at 400–700 °C. The logσ~log(p_{O₂}) curves and fuel cell performances of BaCe_{0.9}Er_{0.1}O_{3-α} and BaCe_{0.9}Er_{0.1}O_{3-α}-K₂SO₄-BaSO₄ were tested at 700 °C. The maximum output power density of BaCe_{0.9}Er_{0.1}O_{3-α}-K₂SO₄-BaSO₄ was 115.9 mW·cm⁻² at 700 °C, which is ten times higher than that of BaCe_{0.9}Er_{0.1}O_{3-α}.

Keywords: composite; fuel cell; BaCeO₃; conductivity; electrolyte

1. Introduction

With the rapid development of the economy, energy problems are imminent. As one of the new energy sources, fuel cells are of great significance. Solid oxide fuel cells (SOFCs) have the advantages of high conversion efficiency, small size, no noise, reduced pollution, and so on [1–8]. However, higher operating temperatures often lead to serious performance degradation, longer start-up times and expensive interconnecting sealing materials, which are considered the main obstacles to SOFCs' commercialization. Therefore, it is urgent to explore SOFCs operating at intermediate temperatures (400–700 °C) and at high performance at the same time. Compared with oxygen ion-conductive SOFCs, proton-conducting SOFCs can operate at lower temperatures. An exploration of electrolyte materials with high protonic conductivities at 400–700 °C is of vital importance [9–14].

It is known that BaCeO₃-based ceramics have good protonic conductivities at high temperatures (700–1000 °C) [15–24]. Using an electrolyte film and a composite electrolyte are two main ways to apply BaCeO₃-based ceramics to intermediate-temperature SOFCs [25–33]. Tong and O'Hayre fabricated five different types of H₂/air fuel cells using BaCe_{0.7}Zr_{0.1}Y_{0.1}Yb_{0.1}O_{3-δ} (BCZY_{Yb}), BaCe_{0.6}Zr_{0.3}Y_{0.1}O_{3-δ} (BCZY63) and BaZr_{0.8}Y_{0.2}O_{3-δ} (BZY20) as electrolytes [26]. Liu et al. reported that a 30 wt.% In³⁺-doped barium cerate–70 wt.% Gd_{0.1}Ce_{0.9}O_{2-δ} composite electrolyte had a high conductivity of 3.42 × 10⁻² S·cm⁻¹ in wet hydrogen at 700 °C [27]. The conductivities of barium cerate-ceria-type composite electrolytes are similar to those of BaCeO₃ doped with low-valent metal cations [27–29]. Park et al. investigated BaZr_{0.85}Y_{0.15}O_{3-δ} (BZY)-carbonate composite electrolytes, which had good

intermediate-temperature electrochemical properties [32]. The literature has mainly focused on reporting carbonate [30–33] and chloride [34–36] composite electrolytes. Only a small number of reports on cerium dioxide–sulfate composite electrolytes have been reported [37]. It is well known that the stability of carbonate is weaker than that of sulfate. Until now, no literature has reported on the barium cerate–sulphate composite electrolyte.

In this study, we synthesized $\text{BaCe}_{0.9}\text{Er}_{0.1}\text{O}_{3-\alpha}$ by a microemulsion method. Then, a $\text{BaCe}_{0.9}\text{Er}_{0.1}\text{O}_{3-\alpha}\text{-K}_2\text{SO}_4\text{-BaSO}_4$ composite electrolyte was obtained by compounding it with a $\text{K}_2\text{SO}_4\text{-Li}_2\text{SO}_4$ solid solution. The characterization and intermediate-temperature (400–700 °C) electrochemical properties of $\text{BaCe}_{0.9}\text{Er}_{0.1}\text{O}_{3-\alpha}$ and $\text{BaCe}_{0.9}\text{Er}_{0.1}\text{O}_{3-\alpha}\text{-K}_2\text{SO}_4\text{-BaSO}_4$ were investigated.

2. Experimental

$\text{BaCe}_{0.9}\text{Er}_{0.1}\text{O}_{3-\alpha}$ was prepared by a microemulsion method. Firstly, Er_2O_3 was completely dissolved with concentrated nitric acid. Sixty milliliters of water was added to make $\text{Ba}(\text{CH}_3\text{COO})_2$ and $(\text{NH}_4)_2\text{Ce}(\text{NO}_3)_6$ dissolve evenly. A mixture of cyclohexane, ethanol and polyvinyl alcohol (PVA) was added to the solution and stirred until it was completely emulsified to form Microemulsion A. Then, $(\text{NH}_4)_2\text{CO}_3$, NH_4OH , cyclohexane, ethanol and PVA were mixed evenly to form Microemulsion B [38,39]. Microemulsion B was slowly added to Microemulsion A. In the process of dropping, the number of white precipitates increased, and a large number of bubbles emerged at the same time. The precipitation was filtered and dried under an infrared lamp to obtain the precursor powder. Finally, the precursor was calcined in a high-temperature furnace at 1250 and 1550 °C for 6 h to obtain $\text{BaCe}_{0.9}\text{Er}_{0.1}\text{O}_{3-\alpha}$.

In this experiment, molten $\text{K}_2\text{SO}_4\text{-Li}_2\text{SO}_4$ (1:1 mole ratio) was prepared in a muffle oven at 750 °C for 2 h [40]. Our previous studies indicated that the stability of 70 wt.% $\text{SrCe}_{0.9}\text{Yb}_{0.1}\text{O}_{3-\alpha}\text{-30 wt.}\%$ (Na/K)Cl was lower, though its conductivities were higher than 80 wt.% $\text{SrCe}_{0.9}\text{Yb}_{0.1}\text{O}_{3-\alpha}\text{-20 wt.}\%$ (Na/K)Cl [41]. Therefore, the $\text{BaCe}_{0.9}\text{Er}_{0.1}\text{O}_{3-\alpha}$ powders were evenly mixed with molten $\text{K}_2\text{SO}_4\text{-Li}_2\text{SO}_4$ powders in a weight proportion of 80%:20%. After being sieved and pressed, the disks were put into the muffle furnace heated at 750 °C for 2 h to obtain $\text{BaCe}_{0.9}\text{Er}_{0.1}\text{O}_{3-\alpha}\text{-K}_2\text{SO}_4\text{-BaSO}_4$.

$\text{BaCe}_{0.9}\text{Er}_{0.1}\text{O}_{3-\alpha}$ and $\text{BaCe}_{0.9}\text{Er}_{0.1}\text{O}_{3-\alpha}\text{-K}_2\text{SO}_4\text{-BaSO}_4$ were characterized by an X-ray diffractometer (XRD, X'pert Pro MPD, Holland's company, Amsterdam, Netherlands), a confocal-micro Raman spectrometer (invia, Renishaw, Gloucestershire, United Kingdom), and a scanning electron microscope (SEM, S-4700, Hitachi, Tokyo, Japan). The Ba, Ce, Er, O, K and S elements in $\text{BaCe}_{0.9}\text{Er}_{0.1}\text{O}_{3-\alpha}\text{-K}_2\text{SO}_4\text{-BaSO}_4$ were measured by the energy-dispersive X-ray spectroscopy.

For intermediate-temperature electrochemical properties, $\text{BaCe}_{0.9}\text{Er}_{0.1}\text{O}_{3-\alpha}$ and $\text{BaCe}_{0.9}\text{Er}_{0.1}\text{O}_{3-\alpha}\text{-K}_2\text{SO}_4\text{-BaSO}_4$ were polished to a thickness of 1.0 mm. Circles 8 mm in diameter were drawn in the center of both sides of the discs with a pencil, and a 20%Pd–80%Ag paste was coated on the circles (area: 0.5 cm²). AC impedance spectroscopy was measured in a nitrogen atmosphere at 400–700 °C. The frequency ranged from 1 to 10⁵ Hz, and the signal voltage was 0.05 V. The $\log\sigma\text{-}\log(p_{\text{O}_2})$ curves of $\text{BaCe}_{0.9}\text{Er}_{0.1}\text{O}_{3-\alpha}$ and $\text{BaCe}_{0.9}\text{Er}_{0.1}\text{O}_{3-\alpha}\text{-K}_2\text{SO}_4\text{-BaSO}_4$ were tested by adjusting different proportions of air, nitrogen, oxygen and hydrogen at room temperature ($p_{\text{H}_2\text{O}} = 2.3 \times 10^3 - 3.1 \times 10^3$ Pa). The two sides of $\text{BaCe}_{0.9}\text{Er}_{0.1}\text{O}_{3-\alpha}$ and $\text{BaCe}_{0.9}\text{Er}_{0.1}\text{O}_{3-\alpha}\text{-K}_2\text{SO}_4\text{-BaSO}_4$ were in hydrogen and oxygen atmospheres, respectively, which constituted the following fuel cells: H_2 , Pd–Ag | sample | Pd–Ag, O_2 . We then measured their $I\text{-}V\text{-}P$ curves.

3. Results and Discussion

Figure 1 is the XRD spectra of $\text{BaCe}_{0.9}\text{Er}_{0.1}\text{O}_{3-\alpha}$ (1250 and 1550 °C) and $\text{BaCe}_{0.9}\text{Er}_{0.1}\text{O}_{3-\alpha}\text{-K}_2\text{SO}_4\text{-BaSO}_4$. The diffraction peaks of $\text{BaCe}_{0.9}\text{Er}_{0.1}\text{O}_{3-\alpha}$ (1250 and 1550 °C) correspond to the standard diagram of BaCeO_3 (JCPDS 85-2155). Neither of the two samples detected Er_2O_3 , which indicates that they had entered the lattice of perovskite phase. In $\text{BaCe}_{0.9}\text{Er}_{0.1}\text{O}_{3-\alpha}$ (1250 °C), in addition to the perovskite phase, there was a very small amount of the CeO_2 phase, indicating the initial calcination temperature should be raised to 1300 or 1350 °C [22]. The weak alkali

salt Li_2SO_4 reacted with the strong base BaO to form BaSO_4 when $\text{BaCe}_{0.9}\text{Er}_{0.1}\text{O}_{3-\alpha}$ powders were mixed with molten sulphate, as indicated by the equation: $\text{BaO} + \text{Li}_2\text{SO}_4 = \text{BaSO}_4 + \text{Li}_2\text{O}$. CeO_2 may be separated from the perovskite structure when sulphate and $\text{BaCe}_{0.9}\text{Er}_{0.1}\text{O}_{3-\alpha}$ form a composite electrolyte. This is why CeO_2 also appears in $\text{BaCe}_{0.9}\text{Er}_{0.1}\text{O}_{3-\alpha}\text{-K}_2\text{SO}_4\text{-BaSO}_4$.

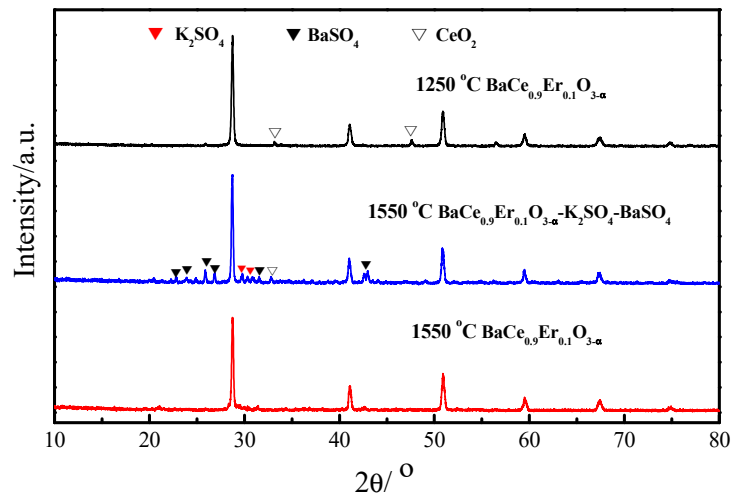


Figure 1. XRD patterns of $\text{BaCe}_{0.9}\text{Er}_{0.1}\text{O}_{3-\alpha}$ (1250 and 1550 °C) and $\text{BaCe}_{0.9}\text{Er}_{0.1}\text{O}_{3-\alpha}\text{-K}_2\text{SO}_4\text{-BaSO}_4$.

Figure 2a,b shows SEM photos of the external and cross-sectional surfaces of the $\text{BaCe}_{0.9}\text{Er}_{0.1}\text{O}_{3-\alpha}$ (1550 °C) ceramic prepared by the microemulsion method. It can be seen that $\text{BaCe}_{0.9}\text{Er}_{0.1}\text{O}_{3-\alpha}$ (1550 °C) had a compact structure, complete grain growth, clear grain boundaries, and very few holes. The density of the $\text{BaCe}_{0.9}\text{Er}_{0.1}\text{O}_{3-\alpha}$ (1550 °C) ceramic prepared by the microemulsion method was higher than that by the high-temperature solid-state method at the same sintering temperature. After adding sulphate, the boundaries between grains became not particularly distinct. There were different degrees of adhesion between grains [32,33]. This is due to the $\text{BaCe}_{0.9}\text{Er}_{0.1}\text{O}_{3-\alpha}$ grains being wrapped in molten sulfate.

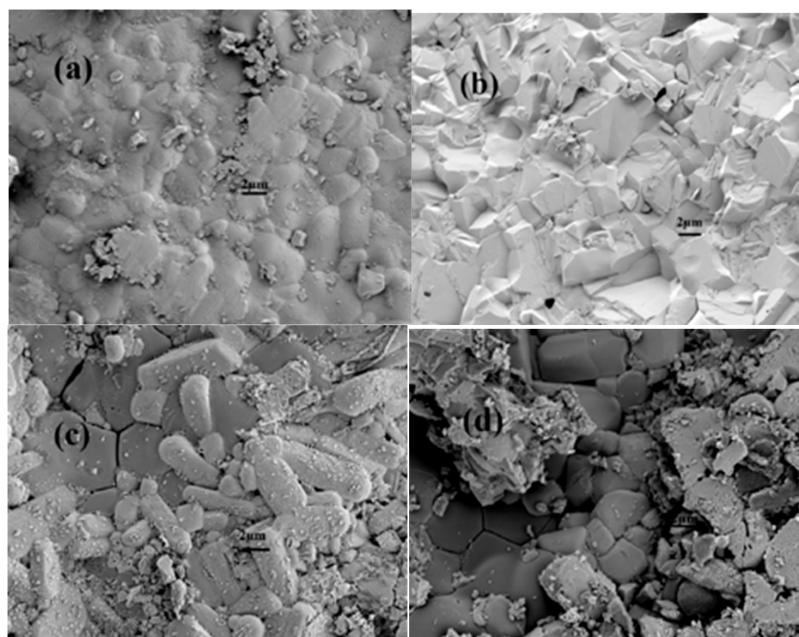


Figure 2. The external (a,c) and cross-sectional (b,d) SEM photos of $\text{BaCe}_{0.9}\text{Er}_{0.1}\text{O}_{3-\alpha}$ (1550 °C) and $\text{BaCe}_{0.9}\text{Er}_{0.1}\text{O}_{3-\alpha}\text{-K}_2\text{SO}_4\text{-BaSO}_4$.

The energy-dispersive X-ray spectroscopy result of $\text{BaCe}_{0.9}\text{Er}_{0.1}\text{O}_{3-\alpha}-\text{K}_2\text{SO}_4-\text{BaSO}_4$ is shown in Figure 3. The spectrum had major peaks assigned to the Ba, Ce, Er, O, K and S elements. The atomic ratios of Ba/Ce, Ba/Er and S/K are 0.87, 9.21 and 1.54. The low content of the Ba element may be due to the formation of BaSO_4 by the reaction: $\text{BaO} + \text{Li}_2\text{SO}_4 = \text{BaSO}_4 + \text{Li}_2\text{O}$, resulting in segregation. The elements mapping images indicated that the spatial distribution of sulphate was uniform.

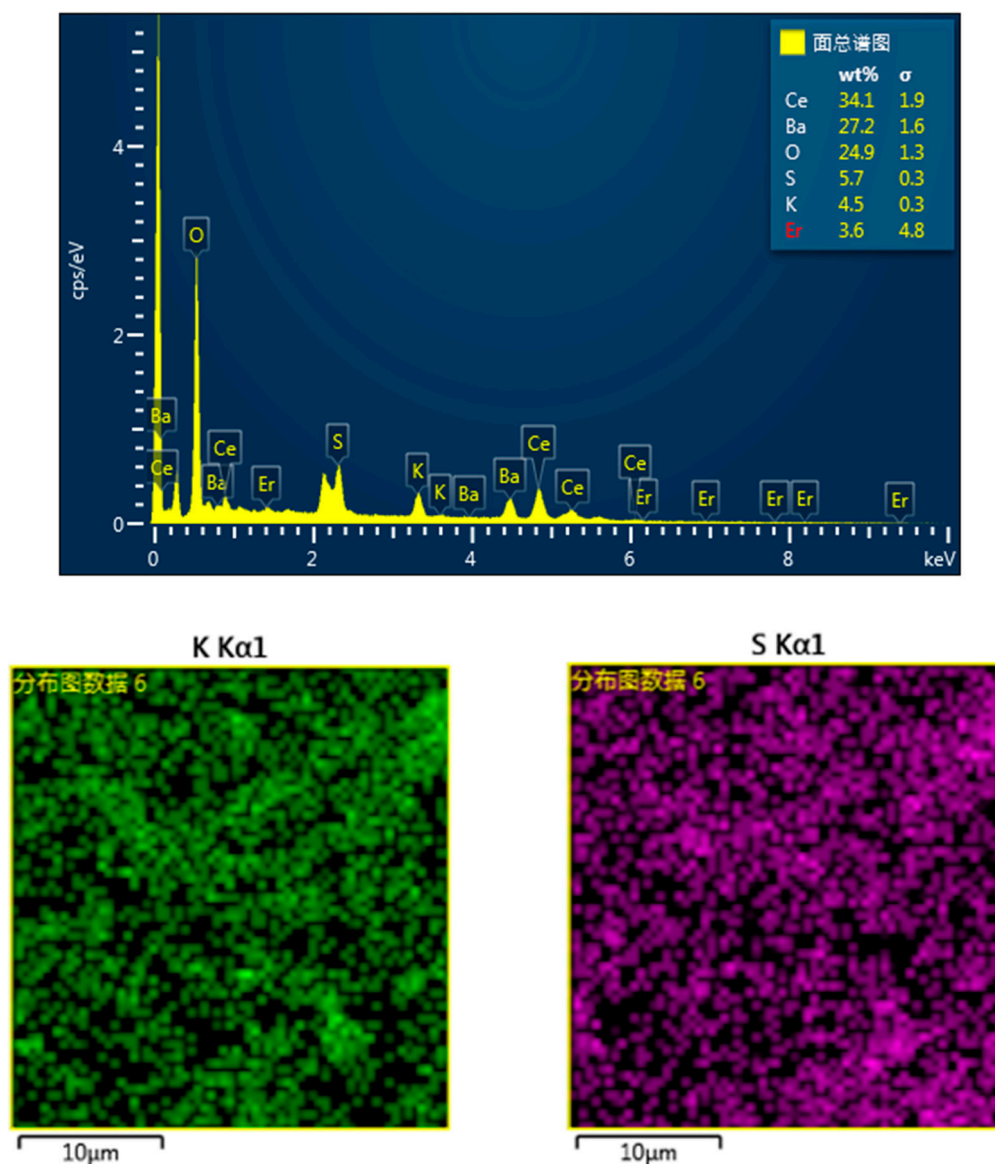


Figure 3. The energy-dispersive X-ray spectroscopy and elements mapping images in $\text{BaCe}_{0.9}\text{Er}_{0.1}\text{O}_{3-\alpha}-\text{K}_2\text{SO}_4-\text{BaSO}_4$.

Figure 4 shows the Raman spectra of $\text{BaCe}_{0.9}\text{Er}_{0.1}\text{O}_{3-\alpha}$ (1550 °C) and $\text{BaCe}_{0.9}\text{Er}_{0.1}\text{O}_{3-\alpha}-\text{K}_2\text{SO}_4-\text{BaSO}_4$. In $\text{BaCe}_{0.9}\text{Er}_{0.1}\text{O}_{3-\alpha}$ (1550 °C), Raman activity peaked around 653 and 723 cm^{-1} , corresponding to the O_h vibrational mode and Ce–O vertical bending vibration in the A_{1g} mode, respectively. In $\text{BaCe}_{0.9}\text{Er}_{0.1}\text{O}_{3-\alpha}-\text{K}_2\text{SO}_4-\text{BaSO}_4$, the Raman peaks near 353, 520, 987 and 1120 cm^{-1} were attributed to S–O bending, bending deformation, symmetrical stretching and antisymmetric telescopic vibration, respectively [38,42–44].

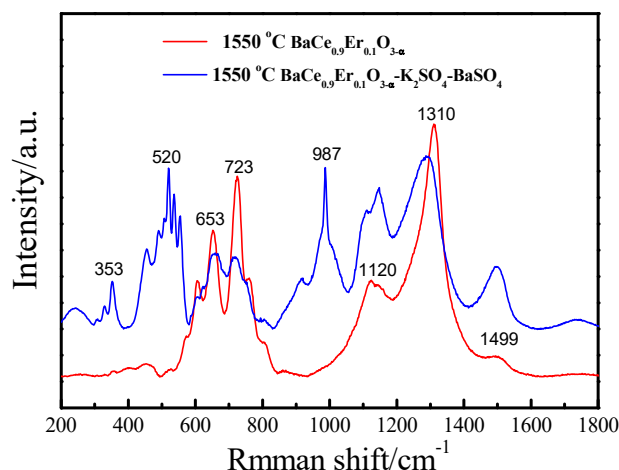


Figure 4. Raman spectra of $\text{BaCe}_{0.9}\text{Er}_{0.1}\text{O}_{3-\alpha}$ (1550 °C) and $\text{BaCe}_{0.9}\text{Er}_{0.1}\text{O}_{3-\alpha}\text{-K}_2\text{SO}_4\text{-BaSO}_4$.

Figure 5 shows the conductivities of $\text{BaCe}_{0.9}\text{Er}_{0.1}\text{O}_{3-\alpha}$ (1550 °C) and $\text{BaCe}_{0.9}\text{Er}_{0.1}\text{O}_{3-\alpha}\text{-K}_2\text{SO}_4\text{-BaSO}_4$ in nitrogen measured from 400 to 700 °C. It can be seen from Figure 5 that the $\text{BaCe}_{0.9}\text{Er}_{0.1}\text{O}_{3-\alpha}\text{-K}_2\text{SO}_4\text{-BaSO}_4$ had a beneficial effect on conductivity. With the addition of sulphate, the conductivity was significantly improved. This is because the sulphate distributed at the grain boundary and formed a continuous phase, so both the main phase and the grain boundary phase could conduct ions. The highest conductivities of $\text{BaCe}_{0.9}\text{Er}_{0.1}\text{O}_{3-\alpha}$ (1550 °C) and $\text{BaCe}_{0.9}\text{Er}_{0.1}\text{O}_{3-\alpha}\text{-K}_2\text{SO}_4\text{-BaSO}_4$ achieved were 9.4×10^{-3} and $1.8 \times 10^{-1} \text{ S}\cdot\text{cm}^{-1}$ at 700 °C. Under the same conditions, the conductivity of $\text{BaCe}_{0.9}\text{Er}_{0.1}\text{O}_{3-\alpha}\text{-K}_2\text{SO}_4\text{-BaSO}_4$ was higher than that of $\text{BaCe}_{0.7}\text{In}_{0.3}\text{O}_{3-\delta}\text{-Gd}_{0.1}\text{Ce}_{0.9}\text{O}_{2-\delta}$ [27] and comparable to values of $\text{BaCe}_{0.83}\text{Y}_{0.17}\text{O}_{3-\delta}\text{-Sm}_{0.15}\text{Ce}_{0.85}\text{O}_{2-\delta}$ [29]. This indicated that the sulphate was conducive to the conduction of ion defects through the interface region in the $\text{BaCe}_{0.9}\text{Er}_{0.1}\text{O}_{3-\alpha}\text{-K}_2\text{SO}_4\text{-BaSO}_4$ composite electrolyte. The conductivity of $\text{BaCe}_{0.9}\text{Er}_{0.1}\text{O}_{3-\alpha}$ was equivalent to that of $\text{BaCe}_{0.7}\text{In}_{0.15}\text{Ta}_{0.05}\text{Y}_{0.1}\text{O}_{3-\delta}$ [22] and $\text{BaCe}_{0.5}\text{Zr}_{0.3}\text{Y}_{0.2-x}\text{Yb}_x\text{O}_{3-\delta}$ in wet H_2 (~3% H_2O) [18]. This may be related to its high density, as shown in Figure 3.

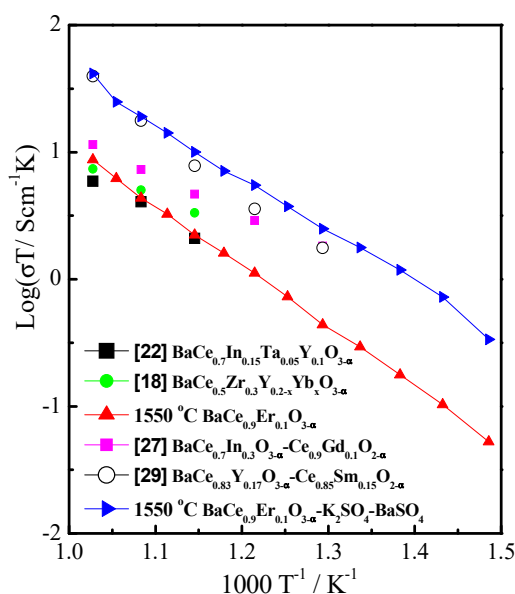


Figure 5. The conductivities of $\text{BaCe}_{0.9}\text{Er}_{0.1}\text{O}_{3-\alpha}$ (1550 °C) and $\text{BaCe}_{0.9}\text{Er}_{0.1}\text{O}_{3-\alpha}\text{-K}_2\text{SO}_4\text{-BaSO}_4$ in nitrogen from 400 to 700 °C.

The conduction characteristics of $\text{BaCe}_{0.9}\text{Er}_{0.1}\text{O}_{3-\alpha}$ and $\text{BaCe}_{0.9}\text{Er}_{0.1}\text{O}_{3-\alpha}\text{-K}_2\text{SO}_4\text{-BaSO}_4$ were tested by adjusting different proportions of gases. As seen in Figure 6, the conductivities of the samples in a reductive atmosphere are very close to those in an oxidizing atmosphere. The $\log\sigma\text{-}\log(p_{\text{O}_2})$ curves of $\text{BaCe}_{0.9}\text{Er}_{0.1}\text{O}_{3-\alpha}$ and $\text{BaCe}_{0.9}\text{Er}_{0.1}\text{O}_{3-\alpha}\text{-K}_2\text{SO}_4\text{-BaSO}_4$ were almost horizontal straight lines. When the temperature exceeded the melting point of sulphate salts, the mobility of various ions (Ba^{2+} , Li^+ , K^+ , H^+) was greatly enhanced, which led to a low activation energy for ion transport in the interface regions. The proton was the smallest cation, and the mobility of protons was greater than other ions (Li^+ , K^+), resulting in an increased conductivity. Therefore, ion conduction appeared to become dominant [34].

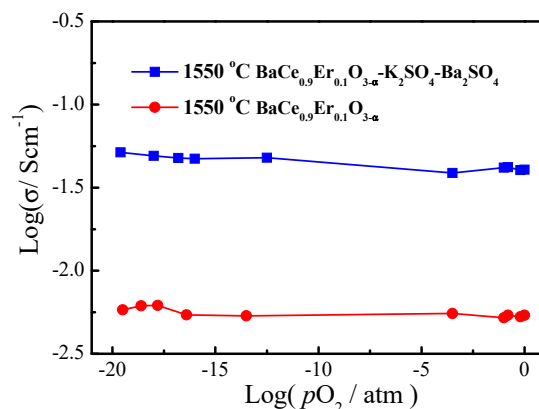


Figure 6. The $\log\sigma\text{-}\log(p_{\text{O}_2})$ curves of $\text{BaCe}_{0.9}\text{Er}_{0.1}\text{O}_{3-\alpha}$ and $\text{BaCe}_{0.9}\text{Er}_{0.1}\text{O}_{3-\alpha}\text{-K}_2\text{SO}_4\text{-BaSO}_4$ at 700 °C.

Hydrogen/oxygen fuel cells were assembled with $\text{BaCe}_{0.9}\text{Er}_{0.1}\text{O}_{3-\alpha}$ and $\text{BaCe}_{0.9}\text{Er}_{0.1}\text{O}_{3-\alpha}\text{-K}_2\text{SO}_4\text{-BaSO}_4$ as supporting electrolytes and Pd–Ag as electrodes. The current–voltage characteristic curves are shown in Figure 7. The resistance directed from current–voltage characteristic curve of $\text{BaCe}_{0.9}\text{Er}_{0.1}\text{O}_{3-\alpha}\text{-K}_2\text{SO}_4\text{-BaSO}_4$ ($2.76\ \Omega$) was lower than that of the value ($5.54\ \Omega$) from AC impedance at 700 °C, implying that the protonic conduction was dominant under the fuel cell condition [45]. The maximum power density of $\text{BaCe}_{0.9}\text{Er}_{0.1}\text{O}_{3-\alpha}$ was $10.9\ \text{mW}\cdot\text{cm}^{-2}$ at 700 °C. Because the fuel cell was supported by the electrolyte and the electrolyte was thicker (1.0 mm), the current and power density were relatively low. When the voltage was 0.6 V, the maximum output power density of $\text{BaCe}_{0.9}\text{Er}_{0.1}\text{O}_{3-\alpha}\text{-K}_2\text{SO}_4\text{-BaSO}_4$ was $115.9\ \text{mW}\cdot\text{cm}^{-2}$ at 700 °C, which is ten times higher than that of $\text{BaCe}_{0.9}\text{Er}_{0.1}\text{O}_{3-\alpha}$. The results show that $\text{BaCe}_{0.9}\text{Er}_{0.1}\text{O}_{3-\alpha}\text{-K}_2\text{SO}_4\text{-BaSO}_4$ is an excellent electrolyte material for medium-temperature fuel cells.

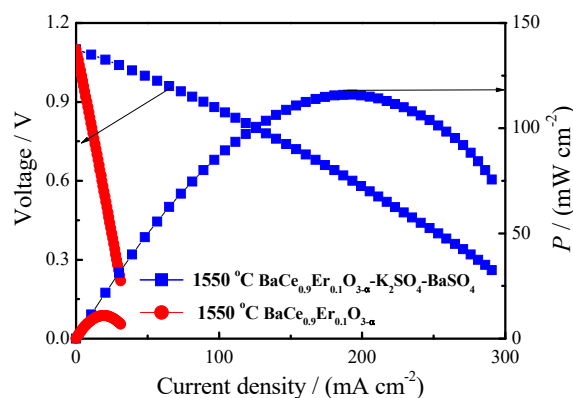


Figure 7. Hydrogen/oxygen fuel cells assembled with $\text{BaCe}_{0.9}\text{Er}_{0.1}\text{O}_{3-\alpha}$ and $\text{BaCe}_{0.9}\text{Er}_{0.1}\text{O}_{3-\alpha}\text{-K}_2\text{SO}_4\text{-BaSO}_4$ as supporting electrolytes at 700 °C.

4. Conclusions

In this study, a $\text{BaCe}_{0.9}\text{Er}_{0.1}\text{O}_{3-\alpha}\text{-K}_2\text{SO}_4\text{-BaSO}_4$ composite electrolyte was obtained by compounding it with a $\text{K}_2\text{SO}_4\text{-Li}_2\text{SO}_4$ solid solution. The XRD diffraction peaks of $\text{BaCe}_{0.9}\text{Er}_{0.1}\text{O}_{3-\alpha}$ (1550 °C) corresponded to the standard diagram of BaCeO_3 , which indicated that Er_2O_3 had entered the lattice of perovskite phase. SEM photos showed the $\text{BaCe}_{0.9}\text{Er}_{0.1}\text{O}_{3-\alpha}$ grains were wrapped in molten sulfate. The highest conductivities of $\text{BaCe}_{0.9}\text{Er}_{0.1}\text{O}_{3-\alpha}$ (1550 °C) and $\text{BaCe}_{0.9}\text{Er}_{0.1}\text{O}_{3-\alpha}\text{-K}_2\text{SO}_4\text{-BaSO}_4$ were 9.4×10^{-3} and $1.8 \times 10^{-1} \text{ S}\cdot\text{cm}^{-1}$ at 700 °C, respectively. The $\log \sigma \sim \log (p/p_{\text{O}_2})$ curves of $\text{BaCe}_{0.9}\text{Er}_{0.1}\text{O}_{3-\alpha}$ and $\text{BaCe}_{0.9}\text{Er}_{0.1}\text{O}_{3-\alpha}\text{-K}_2\text{SO}_4\text{-BaSO}_4$ are almost horizontal straight lines, which indicated that ionic conductivity was dominant. The maximum output power density of $\text{BaCe}_{0.9}\text{Er}_{0.1}\text{O}_{3-\alpha}\text{-K}_2\text{SO}_4\text{-BaSO}_4$ was $115.9 \text{ mW}\cdot\text{cm}^{-2}$ at 700 °C, which is ten times higher than that of $\text{BaCe}_{0.9}\text{Er}_{0.1}\text{O}_{3-\alpha}$.

Author Contributions: H.W. and F.W. conceived and designed the experiments; R.D. and T.H. performed the experiments; H.W. and F.W. analyzed the data; H.Z. contributed the used materials and analysis tools; and H.W. wrote the paper.

Funding: This work was supported by the National Natural Science Foundation (No. 51402052, 21602029) of China, The Natural Science Project of Anhui Province (No. KJ2018A0337), Excellent Youth Foundation of Anhui Educational Committee (No. gxyq2018046), The Guangdong Science and Technology Program (2017B030314002), Horizontal cooperation project of Fuyang municipal government and Fuyang Normal University (No. XDHXTD201704, HX2019004000).

Conflicts of Interest: The authors declare no conflicts of interest.

References

1. Faro, M.L.; Trocino, S.; Zignani, S.C.; Italiano, C.; Vita, A.; Aricò, A.S. Study of a solid oxide fuel cell fed with n-dodecane reformat. Part II: Effect of the reformat composition. *Int. J. Hydrog. Energy* **2017**, *42*, 1751–1757. [[CrossRef](#)]
2. Fragiaco, P.; De Lorenzo, G.; Corigliano, O. Performance analysis of an intermediate temperature solid oxide electrolyzer test bench under a $\text{CO}_2\text{-H}_2\text{O}$ feed stream. *Energies* **2018**, *11*, 2276. [[CrossRef](#)]
3. Tian, Y.; Lü, Z.; Guo, X.; Wu, P. Catalytic activity of Ni-YSZ composite as anode for methane oxidation in solid oxide fuel cells. *Int. J. Electrochem. Sci.* **2019**, *14*, 1093–1106. [[CrossRef](#)]
4. Miyake, M.; Matsumoto, S.; Iwami, M.; Nishimoto, S.; Kameshima, Y. Electrochemical performances of $\text{Ni}_{1-x}\text{Cu}_x/\text{SDC}$ cermet anodes for intermediate-temperature SOFCs using syngas fuel. *Int. J. Hydrog. Energy* **2016**, *41*, 13625–13631. [[CrossRef](#)]
5. De Lorenzo, G.; Fragiaco, P. Electrical and thermal analysis of an intermediate temperature IIR-SOFC system fed by biogas. *Energy Sci. Eng.* **2018**, *6*, 60–72. [[CrossRef](#)]
6. Milewski, J.; Wołowicz, M.; Lewandowski, J. Comparison of SOE/SOFC system configurations for a peak hydrogen power plant. *Int. J. Hydrog. Energy* **2017**, *42*, 3498–3509. [[CrossRef](#)]
7. Kim, H.S.; Bae, H.B.; Jung, W.; Chung, S.Y. Manipulation of nanoscale intergranular phases for high proton conduction and decomposition tolerance in BaCeO_3 polycrystals. *Nano. Lett.* **2018**, *18*, 1110–1117. [[CrossRef](#)]
8. Gong, Z.; Sun, W.; Jin, Z.; Miao, L.; Liu, W. Barium- and strontium-containing anode materials toward ceria-based solid oxide fuel cells with high open circuit voltages. *ACS Appl. Energy Mater.* **2018**, *1*, 3521–3528. [[CrossRef](#)]
9. Pikalova, E.; Medvedev, D. Effect of anode gas mixture humidification on the electrochemical performance of the BaCeO_3 -based protonic ceramic fuel cell. *Int. J. Hydrog. Energy* **2016**, *41*, 4016–4025. [[CrossRef](#)]
10. Bae, S.Y.; Park, J.Y.; Lim, H.T. Investigation of electronic transport property and durability of BCY-BZY electrolyte cells using embedded probes. *Electrochim. Acta* **2017**, *236*, 399–407. [[CrossRef](#)]
11. Vilela, C.; Martins, A.P.C.; Sousa, N.; Silvestre, A.J.D.; Figueiredo, F.M.L.; Freire, C.S.R. Poly (bis [2-(methacryloyloxy) ethyl] phosphate)/bacterial cellulose nanocomposites: Preparation, characterization and application as polymer electrolyte membranes. *Appl. Sci.* **2018**, *8*, 1145. [[CrossRef](#)]
12. Xia, C.; Qiao, Z.; Feng, C.; Kim, J.; Wang, B.; Zhu, B. Study on zinc oxide-based electrolytes in low-temperature solid oxide fuel cells. *Materials* **2018**, *11*, 40. [[CrossRef](#)]

13. Fang, X.; Zhu, J.; Lin, Z. Effects of electrode composition and thickness on the mechanical performance of a solid oxide fuel cell. *Energies* **2018**, *11*, 1735. [[CrossRef](#)]
14. Bernuy-Lopez, C.; Rioja-Monllor, L.; Nakamura, T.; Ricote, S.; O'Hayre, R.; Amezcawa, K.; Einarsrud, M.; Grande, T. Effect of cation ordering on the performance and chemical stability of layered double perovskite cathodes. *Materials* **2018**, *11*, 196. [[CrossRef](#)]
15. Sun, H.; Zhang, S.; Li, C.; Rainwater, B.; Liu, Y.; Zhang, L.; Zhang, Y.; Li, C.; Liu, M. Atmospheric plasma-sprayed BaZr_{0.1}Ce_{0.7}Y_{0.1}Yb_{0.1}O_{3-δ} (BZCYb) electrolyte membranes for intermediate-temperature solid oxide fuel cells. *Ceram. Int.* **2016**, *42*, 19231–19236. [[CrossRef](#)]
16. Danilov, N.; Pikalova, E.; Lyagaeva, J.; Antonov, B.; Medvedev, D.; Demin, A.; Tsiakaras, P. Grain and grain boundary transport in BaCe_{0.5}Zr_{0.3}Ln_{0.2}O_{3-δ} (Ln-Y or lanthanide) electrolytes attractive for protonic ceramic fuel cells application. *J. Power Sources* **2017**, *366*, 161–168. [[CrossRef](#)]
17. Xiao, J.; Chen, L.; Yuan, H.; Ji, L.; Xiong, C.; Ma, J.; Zhu, X. Fabrication and characterization of BaZr_{0.1}Ce_{0.7}Y_{0.2}O_{3-δ} based anode supported solid oxide fuel cells by tape casting combined with spray coating. *Mater. Lett.* **2017**, *189*, 192–195. [[CrossRef](#)]
18. Lyagaeva, J.; Vdovin, G.; Hakimova, L.; Medvedev, D.; Demin, A.; Tsiakaras, P. BaCe_{0.5}Zr_{0.3}Y_{0.2-x}Yb_xO_{3-δ} proton-conducting electrolytes for intermediate-temperature solid oxide fuel cells. *Electrochim. Acta* **2017**, *251*, 554–561. [[CrossRef](#)]
19. Wang, W.; Medvedev, D.; Shao, Z. Gas humidification impact on the properties and performance of perovskite-type functional materials in proton-conducting solid oxide cells. *Adv. Funct. Mater.* **2018**, *28*, 1802592. [[CrossRef](#)]
20. Minakshi, M.; Nallathamby, K.; David, R.G.M. Electrochemical characterization of an aqueous lithium rechargeable battery: The effect of CeO₂ additions to the MnO₂ cathode. *J. Alloy Compd.* **2009**, *479*, 87–90. [[CrossRef](#)]
21. Sun, L.; Miao, H.; Wang, H. Novel SrCe_{1-x}Yb_xO_{3-α}-(Na/K)Cl composite electrolytes for intermediate temperature solid oxide fuel cells. *Solid State Ions.* **2017**, *311*, 41–45. [[CrossRef](#)]
22. Zhang, Z.; Chen, L.; Li, Q.; Song, T.; Su, J.; Cai, B.; He, H. High performance In, Ta and Y-doped BaCeO₃ electrolyte membrane for proton-conducting solid oxide fuel cells. *Solid State Ions.* **2018**, *323*, 25–31. [[CrossRef](#)]
23. Shi, R.; Liu, J.; Wang, H.; Wu, F.; Miao, H.; Cui, Y. Low temperature synthesis of SrCe_{0.9}Eu_{0.1}O_{3-α} by sol-gel method and SrCe_{0.9}Eu_{0.1}O_{3-α}-NaCl-KCl composite electrolyte for intermediate temperature fuel cells. *Int. J. Electrochem. Sci.* **2017**, *12*, 11594–11601. [[CrossRef](#)]
24. Guo, Y.; Liu, B.; Yang, Q.; Chen, C.; Wang, W.; Ma, G. Preparation via microemulsion method and proton conduction at intermediate-temperature of BaCe_{1-x}Y_xO_{3-α}. *Electrochem. Commun.* **2009**, *11*, 153–156. [[CrossRef](#)]
25. Morejudo, S.H.; Zanón, R.; Escolástico, S.; Yuste-Tirados, I.; Malerød-Fjeld, H.; Vestre, P.K.; Coors, W.G.; Martínez, A.; Norby, T.; Serra, J.M.; et al. Direct conversion of methane to aromatics in a catalytic co-ionic membrane reactor. *Science* **2016**, *353*, 563–566. [[CrossRef](#)]
26. Duan, C.; Tong, J.; Shang, M.; Nikodemski, S.; Sanders, M.; Ricote, S.; Almonsoori, A.; O'Hayre, R. Readily processed protonic ceramic fuel cells with high performance at low temperatures. *Science* **2015**, *349*, 1321–1326. [[CrossRef](#)]
27. Liu, F.; Dang, J.; Hou, J.; Qian, J.; Zhu, Z.; Wang, Z.; Liu, W. Study on new BaCe_{0.7}In_{0.3}O_{3-δ}-Gd_{0.1}Ce_{0.9}O_{2-δ} composite electrolytes for intermediate-temperature solid oxide fuel cells. *J. Alloy Compd.* **2015**, *639*, 252–258. [[CrossRef](#)]
28. Park, K.Y.; Lee, T.H.; Jo, S.; Yang, J.; Song, S.J.; Lim, H.T.; Kim, J.H.; Park, J.Y. Electrical and physical properties of composite BaZr_{0.85}Y_{0.15}O_{3-δ}-Nd_{0.1}Ce_{0.9}O_{2-δ} electrolytes for intermediate temperature-solid oxide fuel cells. *J. Power Sources* **2016**, *336*, 437–446. [[CrossRef](#)]
29. Li, B.; Liu, S.; Liu, X.; Qi, S.; Yu, J.; Wang, H.; Su, W. Electrical properties of SDC-BCY composite electrolytes for intermediate temperature solid oxide fuel cell. *Int. J. Hydrog. Energy* **2014**, *39*, 14376–14380. [[CrossRef](#)]
30. Rondao, A.I.B.; Patricio, S.G.; Figueiredo, F.M.L.; Marques, F.M.B. Composite electrolytes for fuel cells: Long-term stability under variable atmosphere. *Int. J. Hydrog. Energy* **2014**, *39*, 5460–5469. [[CrossRef](#)]
31. Martins, N.C.T.; Rajesh, S.; Marques, F.M.B. Synthesis and electrochemical assessment of Ce_{0.5}Yb_{0.5}O_{1.75} ceramics and derived composite electrolytes. *Mater. Res. Bull.* **2015**, *70*, 449–455. [[CrossRef](#)]

32. Park, K.Y.; Lee, T.H.; Kim, J.T.; Lee, N.; Seo, Y.; Song, S.J.; Park, J.Y. Highly conductive barium zirconate-based carbonate composite electrolytes for intermediate temperature-protonic ceramic fuel cells. *J. Alloy Compd.* **2014**, *585*, 103–110. [[CrossRef](#)]
33. Hei, Y.; Huang, J.; Wang, C.; Mao, Z. Novel doped barium cerate-carbonate composite electrolyte material for low temperature solid oxide fuel cells. *Int. J. Hydrog. Energy* **2014**, *39*, 14328–14333. [[CrossRef](#)]
34. Zhang, W.; Yuan, M.; Wang, H.; Liu, J. High-performance intermediate temperature fuel cells of new $\text{SrCe}_{0.9}\text{Yb}_{0.1}\text{O}_{3-\alpha}$ -inorganic salt composite electrolytes. *J. Alloy Compd.* **2016**, *677*, 38–41. [[CrossRef](#)]
35. Shi, R.; Liu, J.; Wang, H.; Wu, F.; Miao, H. Intermediate temperature fuel cell durability of Eu-doped SrCeO_3 - SrZrO_3 solid solution/ NaCl - KCl composite electrolyte. *Ceram. Int.* **2017**, *43*, 16931–16935. [[CrossRef](#)]
36. Slim, C.; Baklouti, L.; Cassir, M.; Ringuedé, A. Structural and electrochemical performance of gadolinia-doped ceria mixed with alkali chlorides (LiCl - KCl) for Intermediate Temperature-Hybrid Fuel Cell applications. *Electrochim. Acta* **2014**, *123*, 127–134. [[CrossRef](#)]
37. Yao, C.; Meng, J.; Liu, X.; Zhang, X.; Liu, X.; Meng, F.; Wu, X.; Meng, J. Enhanced ionic conductivity in Gd-doped ceria and $(\text{Li/Na})_2\text{SO}_4$ composite electrolytes for solid oxide fuel cells. *Solid State Sci.* **2015**, *49*, 90–96. [[CrossRef](#)]
38. Song, J.; Meng, B.; Tan, X. Stability and electrical conductivity of $\text{BaCe}_{0.85}\text{Tb}_{0.05}\text{M}_{0.1}\text{O}_{3-\delta}$ ($\text{M} = \text{Co}, \text{Fe}, \text{Y}, \text{Zr}, \text{Mn}$) high temperature proton conductors. *Ceram. Int.* **2016**, *42*, 13278–13284. [[CrossRef](#)]
39. Reddy, G.S.; Bauri, R. Y and In-doped BaCeO_3 - BaZrO_3 solid solutions: Chemically stable and easily sinterable proton conducting oxides. *J. Alloy Compd.* **2016**, *688*, 1039–1046. [[CrossRef](#)]
40. Liu, X.; Fechler, N.; Antonietti, M. Salt melt synthesis of ceramics, semiconductors and carbon nanostructures. *Chem. Soc. Rev.* **2013**, *42*, 8237–8265. [[CrossRef](#)]
41. Wang, H.; Liu, J. Low temperature synthesis of novel $\text{SrCe}_{0.9}\text{Yb}_{0.1}\text{O}_{3-\alpha}$ -chlorides composite electrolytes for intermediate temperature protonic ceramics fuel cells. *Ceram. Int.* **2016**, *42*, 18136–18140. [[CrossRef](#)]
42. Phokha, S.; Hunpratub, S.; Usher, B.; Pimsawat, A.; Chanlek, N.; Maensiri, S. Effects of CeO_2 nanoparticles on electrochemical properties of carbon/ CeO_2 composites. *Appl. Surf. Sci.* **2018**, *446*, 36–46. [[CrossRef](#)]
43. Preethi, S.; Abhiroop, M.; Babu, K.S. Low temperature densification by lithium co-doping and its effect on ionic conductivity of samarium doped ceria electrolyte. *Ceram. Int.* **2019**, *45*, 5819–5828. [[CrossRef](#)]
44. Hou, Y.; Wu, J.; Konyshva, E.Y. Quantitative characterization of Cr-adsorption on CeO_2 , pure and doped BaCeO_3 and its impact on the electrochemical performance of Ce containing complex oxides. *Int. J. Hydrog. Energy* **2016**, *41*, 3994–4004. [[CrossRef](#)]
45. Huang, J.; Mao, Z.; Liu, Z.; Wang, C. Performance of fuel cells with proton-conducting ceria-based composite electrolyte and nickel-based electrodes. *J. Power Sources* **2008**, *175*, 238–243. [[CrossRef](#)]

